Chapter 15
Impact of Environmental Factors on Polymeric Films Used in Protective Glazing Systems

Kar Tean Tan, Christopher White, Donald Hunston, Aaron Forster, Deborah Stanley, Amy Langhorst, and Patrick Gaume

Abstract Accelerated and natural aging of safety films used in protective glazing systems was investigated by the use of Fourier transform infrared spectroscopy (FTIR), ultraviolet–visible spectroscopy, and tensile tests. Accelerated conditions involved simultaneous exposure of specimens to ultraviolet (UV) radiation between 295 and 450 nm and each of four temperature/relative humidity (RH) environments, i.e., (a) 30 °C at <1 % RH, (b) 30 °C at 80 % RH, (c) 55 °C at <1 % RH, and (d) 55 °C at 80 % RH. Outdoor weathering was performed in Gaithersburg, MD, in two different time periods. FTIR spectra indicate that different exposure conditions have no consequence on the nature and the proportions of the oxidation products, suggesting that similar degradation mechanisms were operative under all outdoor and indoor conditions. In the accelerated exposure, the rate of degradation is found to be influenced dominantly by UV radiation. The combination of UV radiation and temperature results in a cumulative effect, producing more rapid degradation. Analogous to the chemical changes, post-yield mechanical behaviors (such as strain hardening modulus and elongation to break) are markedly reduced, while the Young's modulus is minimally affected. Photodegradation leads finally to instability in the polymer's necking behavior and embrittlement, which is explained in terms of chain scissions of the tie molecules in the amorphous region. Samples subjected to outdoor weathering exhibit significantly slower photodegradation, but the degradation mechanism is the same so higher doses of environmental factors can be used to provide reliable acceleration in short-term aging tests.

K.T. Tan
Engineering Laboratory, National Institute of Standards and Technology, Gaithersburg, MD 20899, USA

Department of Materials Science and Engineering, University of Maryland, College Park, MD 20742, USA

C. White (✉) • D. Hunston • A. Forster • D. Stanley • A. Langhorst • P. Gaume
Engineering Laboratory, National Institute of Standards and Technology, Gaithersburg, MD 20899, USA
e-mail: christopher.white@nist.gov

C.C. White et al. (eds.), *Service Life Prediction of Exterior Plastics: Vision for the Future*, DOI 10.1007/978-3-319-06034-7_15

Keywords Safety films • Protective glazing • Degradation • Glass • Blast resistance • Polyetheyleneteraphthalate • PET • Outdoor exposure • Weathering

Introduction

Traditional annealed window glass may implode at high velocities producing jagged shards when subjected to blast pressures that resulted from natural disasters (e.g., hurricanes, tornadoes, severe wind storms, and seismic activities) or man-made destructions (e.g., burglary, vandalism, terrorist bombings, and industrial explosions). Flying glass shards pose significant risks to building occupants and can generate major damage to properties. This can be seen in a series of tornados that recently ravaged Alabama and the mid-west where destruction or damage of glazing caused serious injuries and property damage. To prevent glass shards from becoming lethal projectiles, polymeric films (known as safety films) are applied to window glass. During failure, the safety films deform to absorb energy that causes the glass to break as well as to keep broken glass shards adhered to the films. Thus, the blast load can be transferred to a building's frame and shattered glass fragments do not exit from windows at high velocities.

A variety of test methods and specifications are used to evaluate and validate the initial performance of safety films and glazing systems. These include ASTM F1642 (Standard Test Method for Glazing and Glazing Systems Subject to Air blast Loadings), ASTM F1233 (Standard Test Method for Security Glazing Materials and Systems), ISO 16933 Glass in Building—explosion-resistant security glazing—Test and Classification for Arena Air-Blast loading, and AAMA 510-06 (Voluntary Guide Specification for Blast Hazard Mitigation for Fenestration Systems). While helpful in assessing the initial material performance, these standard tests do not address an important question concerning the long-term chemical and mechanical stability of the film. It is well known that ultraviolet (UV) radiation, moisture, or extreme temperature can all contribute to the deterioration of material properties of polymer films, and this potentially shortens their useful life spans [1, 2]. Furthermore, the service life predictive capabilities for safety films are still far from being satisfactory both from the analytical and experimental points of view. A better understanding of degradation mechanics and mechanisms is key to accurately predict service life and develop products with improved long-term performance. The work here seeks to provide a fundamental understanding of the degradation mechanism for safety films exposed to various environmental factors and to clarify the effect of each environmental factor on the degradation mechanisms. Accelerated aging tests were conducted in an integrating sphere-based weathering chamber [Simulated Photodegradation via High Energy Radiant Exposure (SPHERE)] [3]. Changes in key mechanical and chemical properties as a function of exposure time at different temperatures and moisture levels during accelerated aging were measured using quasi-static tensile tests, Fourier transform infrared (FTIR) spectroscopy, and ultraviolet–visible spectroscopy. In addition, a

linkage between accelerated tests and field exposure experiments was established to provide the key that makes the accelerated testing methodology meaningful. This understanding of the degradation with various exposure factors will open new perspective for the practical long-term applications of safety films.

Experimental[1]

Materials

Two commercial safety films were investigated, both of which were obtained from their primary manufacturers. These materials are typical poly(ethylene terephthalates) (PET), but the detailed product chemistry and composition are unknown. Both are manufactured with multiple layers of optically clear films and are installed by attachment to the interior surface of the glass using a pressure-sensitive adhesive. Hereafter, they are referred to as Films A and B, respectively. The films are used as received from the manufacturers.

Accelerated and Field Exposures

Specimens were exposed to both outdoor (field) conditions and indoor experiments where the conditions were designed to accelerate the effects of exposure. For the indoor tests, the specimens were exposed to UV radiation with wavelengths ranging between 295 and 450 nm using the National Institute of Standards and Technology (NIST) integrating sphere-based weathering chamber (SPHERE) [3]). This chamber provides higher UV irradiation than normal outdoor exposure. In addition to the UV irradiation, specimens were subjected to one of four temperature/relative humidity (RH) environments: (a) 30 ± 1 °C and <1 % RH, (b) 30 ± 1 °C and 75 % RH, (c) 55 ± 1 °C and <1 % RH, and (d) 55 ± 1 °C and 75 % RH. Additionally, similar exposures were also conducted in the absence of UV radiation to examine the influence of that parameter on the material properties.

In the case of field tests, specimens were exposed on the roof of a NIST laboratory in Gaithersburg, MD. Specimens were placed in a custom-built chamber that was positioned facing south toward the equator at an angle of 5° from the horizontal plane. Solar radiation reached the specimens through a borosilicate glass plate at the top of the chamber to emulate the conditions seen in the actual applications of the films. The upper surface of the bottom side of the chamber consisted of a 3 mm

[1] Certain commercial products or equipment are described in this paper in order to specify adequately the experimental procedure. In no case does such identification imply recommendation or endorsement by the National Institute of Standards and Technology (NIST), nor does it imply that it is necessarily the best available for the purpose.

thick polytetrafluoroethylene sheet, which was used to minimize heating in the chamber via reflection of the solar radiation. The sides of the chamber were made with a breathable cloth that allowed transmission of water vapor but prevented dust from entering. The temperature, RH, and total irradiance in the chamber were monitored continuously during exposure using thermocouples, humidity sensors, and a radiometer, respectively.

FTIR Spectroscopy

Surface chemical properties of the specimens were measured using a Nexus 670 attenuated total-reflection Fourier transform infrared spectrometer (ATR-FTIR) equipped with a liquid nitrogen-cooled mercury cadmium telluride detector. All spectra were collected over a range of 1,000–4,000 cm^{-1} at a nominal resolution of 4 cm^{-1} and averaged over 128 scans. Band height was used as a measure of IR intensity. In this study, the carboxyl index was used as an indication for degradation in the materials. This index was determined by normalizing the absorbance of 3,255 cm^{-1} (attributable to OH stretching in carboxylic groups [4]) with a least-changed reference band. This was done to compensate for surface morphological changes during exposure that may produce inconsistent optical contact between the polymer film and the internal reflection element of the ATR cell. The reference peaks selected for Films A and B were 1,453 cm^{-1} (C–H in-plane bending of the benzene ring [5]) and 767 cm^{-1} (corresponds to a monosubstituted benzene [4]), respectively.

Tensile Tests

Mechanical properties were measured by uniaxial tensile tests performed at room temperature using an Instron testing machine. The films were cut to a dog-bone geometry conforming to the ASTM D-638. We first investigated the strain rate dependence of mechanical properties for the fresh films. This was done to establish the appropriate strain rate to be used in the subsequent measurements. It was found that elongation at break, the strain hardening modulus, and small-strain Young's modulus are statistically insensitive to crosshead speeds ranging from 1×10^{-3} mm/s to 8.33 mm/s. This indicates a range of over nearly three decades where the behavior is not sensitive to strain rate so a crosshead speed of 0.1 mm/s was used in all subsequent experimental which kept the duration of the tests within a reasonable timescale. To examine the effects of UV, temperature, and RH, mechanical properties such as strain hardening modulus, elongation at break, and Young's modulus were monitored. Strain hardening modulus was obtained by fitting a straight line to the initial plastic region of the curve, while elongation at break was taken as the value of nominal strains at ultimate failure.

Ultraviolet–Visible Spectroscopy

Ultraviolet–visible spectroscopy was utilized to monitor yellowing in the specimens during exposure. The measurements employed a Perkin-Elmer Lambda 900 Spectrometer. The surface color changes of specimens were quantified with a yellowness index (YI). YI is a measure of the visual yellowing that occurs and is based on determination of transmittances (T) near the ends of the visible wavelength region, i.e., $YI = 100 \times (T_{680} - T_{420})/T_{560}$. Here, the subscript denotes the wavelength.

Results and Discussion

Surface Chemical Property Changes upon Exposure

Surface chemistry of the films exposed to various accelerated conditions was monitored by ATR-FTIR. For simplicity, Fig. 15.1 shows typical spectra before and after exposure to 30 °C and 75 % RH in the presence of UV for various exposure times. The IR spectral properties of Films A and B show marked similarities. The assignments of bands for most PET infrared peaks have been well documented in the literature [6–9]. As compared to control specimens, FTIR analyses at various stages

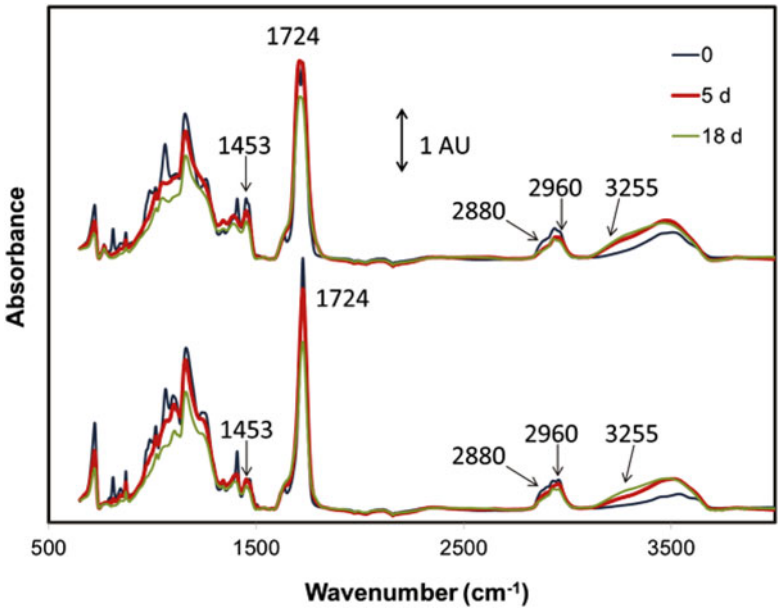

Fig. 15.1 FTIR spectra of Films A (*top*) and B (*bottom*) exposed to 30 °C and 75 % RH. Only three exposure times are shown for clarity

of degradation reveal the appearance of oxidized products on the material surfaces, reflecting structural modifications of the samples under the influence of accelerated exposure conditions. A strong band at 1,724 cm^{-1} due to C=O stretching vibration of the ester groups [6, 10] shows a reduction in intensity with increasing exposure. Similarly, the absorbance of the region around (1,250–1,000) cm^{-1} dominated by strong signals due to C–O stretching vibration [5, 6] shows significant decreases upon exposure.

Examination of the 3,800 cm^{-1} to 3,100 cm^{-1} region (assigned to hydroxyl stretching vibrations) reveals a marked increase in the absorbance of this broad band in the early stage of exposure. The complex line shape of this band suggests that more than one type of bonded OH group is formed. Hydroperoxides (3,550 cm^{-1}) are the main intermediate species present during the early events of the aging process. In later stages, a shoulder was detected at 3,255 cm^{-1}, which may be assigned to OH stretch in carboxylic groups (COOH), and the absorbance of this peak continues to increase with exposure. The absorption bands at 2,960 cm^{-1} and 2,880 cm^{-1} are due to aliphatic C–H stretch [11], while the bands peaking at 1,604, 1,584, 1,492, and 1,453 cm^{-1} stem from C–H in-plane bending of the benzene ring [5]. The intensities of these bands decrease markedly with exposure time. A band at 730 cm^{-1} due to *p*-substituted aromatics [6, 12] also decreases. The reduced absorbance of these bands suggests that extensive degradation has taken place in the films during the exposure. The above FTIR findings are in agreement with the photodegradation mechanisms of PET, which follows Norrish type I reaction pathways, predominantly, and lead to this formation of aldehydes and carboxylic acid [13, 14]. Although not reported here, volatile degradation products such as carbon monoxide and carbon dioxide have been found during the degradation [13, 14].

Figure 15.2 depicts the correlation between the absorbance of two characteristic FTIR bands associated with photooxidation: 1,724 vs. 1,158 cm^{-1} for Films A and B. In such a plot, all of the data for various exposure conditions collapse to a narrow band around a single curve. A direct implication of this good correlation is that the relative proportions of the photooxidation products are independent of the exposure conditions. When the peak ratios show a similar proportionality, various exposure conditions are expected to cause degradation by the same mechanisms, even though the degradation rates are quite different. Thus, the results suggest that the primary mechanism of oxidation in the films does not vary with temperature, RH, and UV.

To evaluate the effects of UV, temperature, and moisture on the kinetics of degradation, changes in carboxyl index were monitored as a function of time (Fig. 15.3). In the presence of UV, the carboxyl index progressively increases with exposure time for all four conditions. Spectra for Film B under conditions of 30 °C/0 % RH and 55 °C/0 % RH reach a plateau in the carboxyl index after $\approx$ 5 days while the increase in carboxyl index for all other conditions slows greatly after $\approx$ 30 days. This suggests saturation of chemical moieties due to the depletion of preferential reaction sites. During the early stages of exposure, various temperature/RH combinations have qualitatively the same effect on the time evolution of carboxyl index. This result indicates that the weak effect of temperature and moisture on degradation may

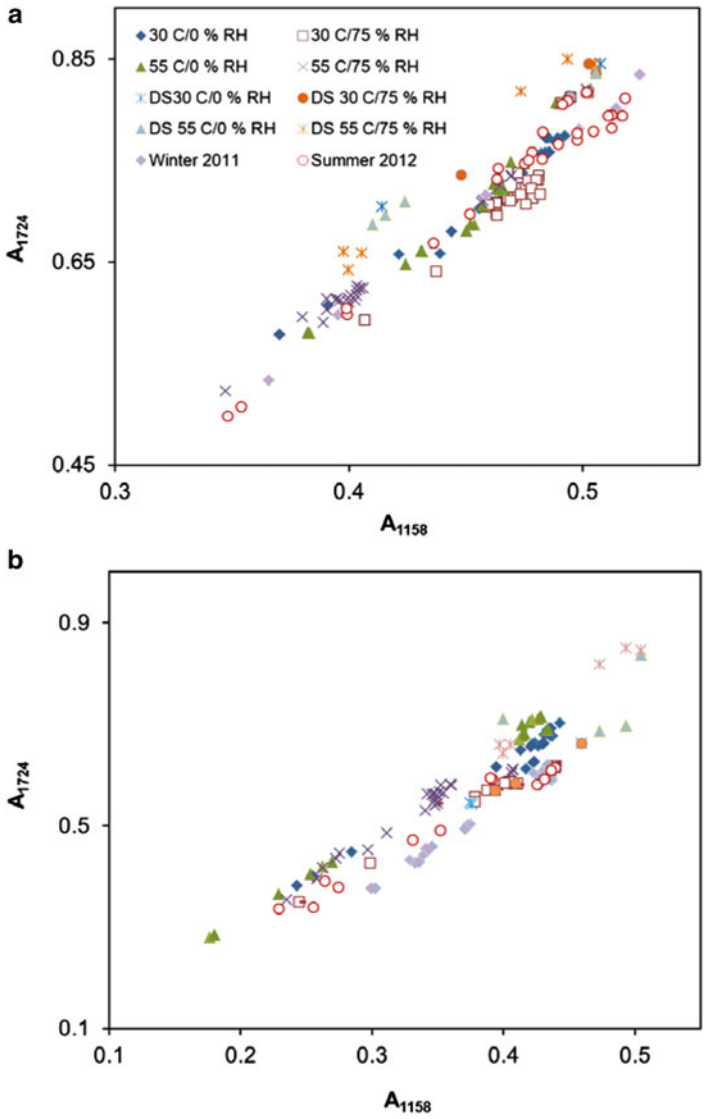

Fig. 15.2 Correlation between absorbance of 1,724 cm^{-1} and 1,158 cm^{-1} for (**a**) Films A and (**b**) B exposed to various conditions. "DS" denotes the exposure without UV radiation. Different exposure conditions have no consequence on the nature and the proportions of the photoproducts, suggesting that similar degradation mechanisms were operative under all outdoor and indoor conditions

be obscured by pronounced effect of UV and that any changes induced by these two factors are too small to be detected with the FTIR spectrometer used here.

In contrast to the early stages of exposure, temperature and moisture begin to affect the oxidation in the films after sufficiently long irradiation time. Distinct

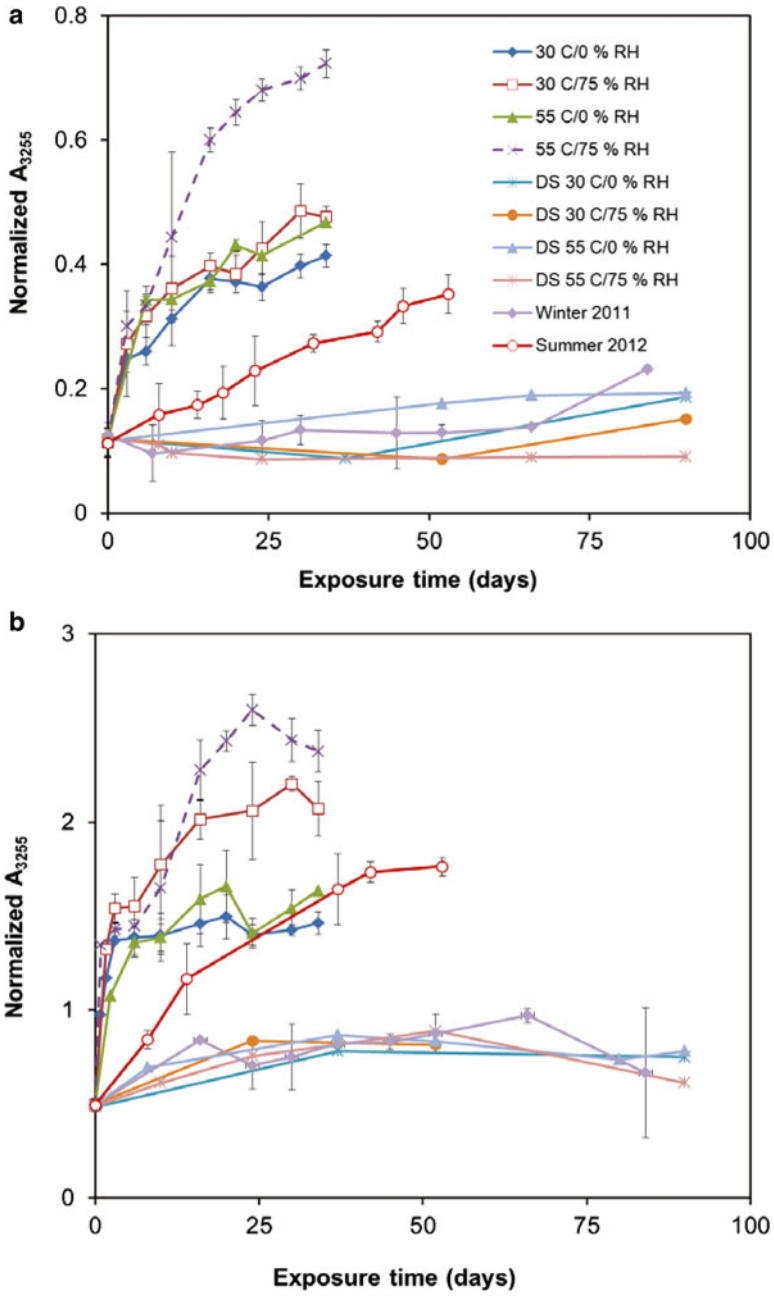

Fig. 15.3 Changes of the normalized absorbance of 3,255 cm^{-1} in (**a**) Films A and (**b**) B as a function of exposure time for different environments. Error bars represent ±1σ from the mean values. "DS" denotes the exposure without UV radiation

dependencies on temperature and moisture were observed in Films A and B. By comparison, the extent of oxidation in Film B shows stronger moisture sensitivity than that in Film A. This is evident from higher carboxyl indexes observed in Film B exposed to a high RH level (i.e., 75 % RH), irrespectively, of temperature. In Film A, the statistically similar carboxyl indexes for 0 % RH and 75 % RH at 30 °C suggest that such a moisture dependency is absent. For exposure at 75 % RH, increasing the temperature results in more noticeable degradation which enriches the carboxyl groups on Films A and B, whereas this effect is barely detectable at the corresponding lower RH levels. Also, the combination of high temperature and RH levels is found to be deleterious for both films. For example, the carboxyl indexes for 55 °C/75 % RH for Films A and B are 70 % greater than that under 30 °C/0 % RH. It should be noted, however, that increasing the temperature from 30 to 55 °C seems insufficient, by itself, to cause any bond ruptures in commercial grade polymers where dissociation energies are 70–90 kcal/mol [15]. Hence, it is the combination of UV, temperature, and moisture that contributes to the observed chemical changes.

The fact that the polymers degrade, as observed in Fig. 15.3, indicates that quanta of light are absorbed by chromophores, which are present as impurities from manufacturing and processing. Additionally, aromatic ester groups in the main chains can readily absorb UV light and thus become a source of the initiation radicals. After absorbing UV radiation, the energy of the excited groups is dissipated via various oxidative mechanisms, leading to the formation of free radicals and various degradation products. Secondary reactions are subsequently promoted by other environmental factors, such as temperature and moisture. This explains the dominance of the UV effect in the initial stage of degradation before the effects of temperature and RH set in the later stages. Further reinforcement for this assertion is given by the largely unaltered carbonyl index measured for the specimens in the absence of UV.

In the literature, it is reported that thermo-oxidative degradation in PET does occur under sufficiently elevated temperatures [16–19]. It is thought to proceed via a scission of in-chain ester linkages, thereby yielding carboxyl and vinyl ester end groups [16–18]. In addition, the degradation process is exacerbated at temperatures above the melting point of the bulk polymer (≈255 °C) [18]. Higher water contents in the polymers at temperatures above the glass transition temperature can damage the polymer directly via hydrolysis, furnishing carboxylic and alcoholic end groups [20]. Such hydrolysis reactions preferentially occur in the amorphous domains of the polymer [21, 22]. Taken together, these various findings suggest that in the absence of UV radiation, the different combinations of temperature and relative humidity utilized in this study are not damaging enough to induce significant degradation in the polymers. This may account for the observed weak dependence of degradation on temperature and RH.

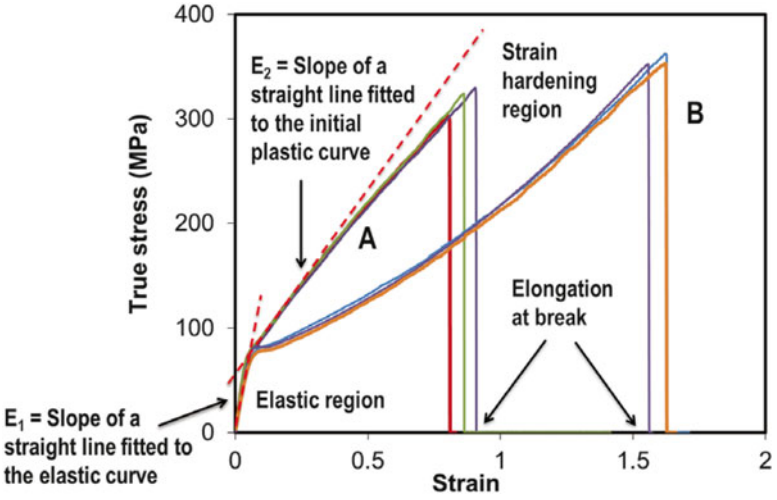

Fig. 15.4 Typical stress versus strain curves for Films A and B

Mechanical Property Changes upon Exposure

It is useful to measure a direct mechanical response of materials under the different exposure conditions. It should be noted that no attempts were made to quantitatively correlate changes in surface chemical and bulk mechanical properties. Figure 15.4 shows representative uniaxial stress–strain curves for fresh Films A and B. Three replicates are presented for each material. In a stress–strain test, Films A and B exhibit comparable features: an initial elastic region followed by yielding which produces a stable necking section that grows until failure occurs at high strains, approximately 80 % for Film A and 160 % for Film B, respectively. The necking region of the curve is characterized by a rise in stress with increasing strain which is termed strain hardening. The high values of elongation at break are indicative for intrinsic ductility of the materials, which makes them attractive for applications where toughness is desired.

Three notable differences between these materials lie at their post-yield regions. First, the previously discussed strain at break values that are 80 % for Film A and 160 % for Film B. Second, Film B shows a moderate region of strain softening (i.e., a drop in the true stress with increasing deformation) prior to the stress hardening. Such a behavior is absent in Film A. Third, the strain hardening slope at moderate deformations is larger in Film A than it is in Film B. Both films exhibit comparable strain hardening rates at large-strain levels. The presence of strain hardening effect reveals the ability of the polymers to undergo plastic flow process involving extensive molecular alignment in the direction of applied load. As a result, the propensity for strain localization is reduced by strong strain hardening. Therefore, the macroscopic response of these materials to large deformation is ductility.

Figures 15.5, 15.6, and 15.7 illustrate how the various exposure conditions impact the elongations at break, Young's moduli, and strain hardening moduli of the specimens.

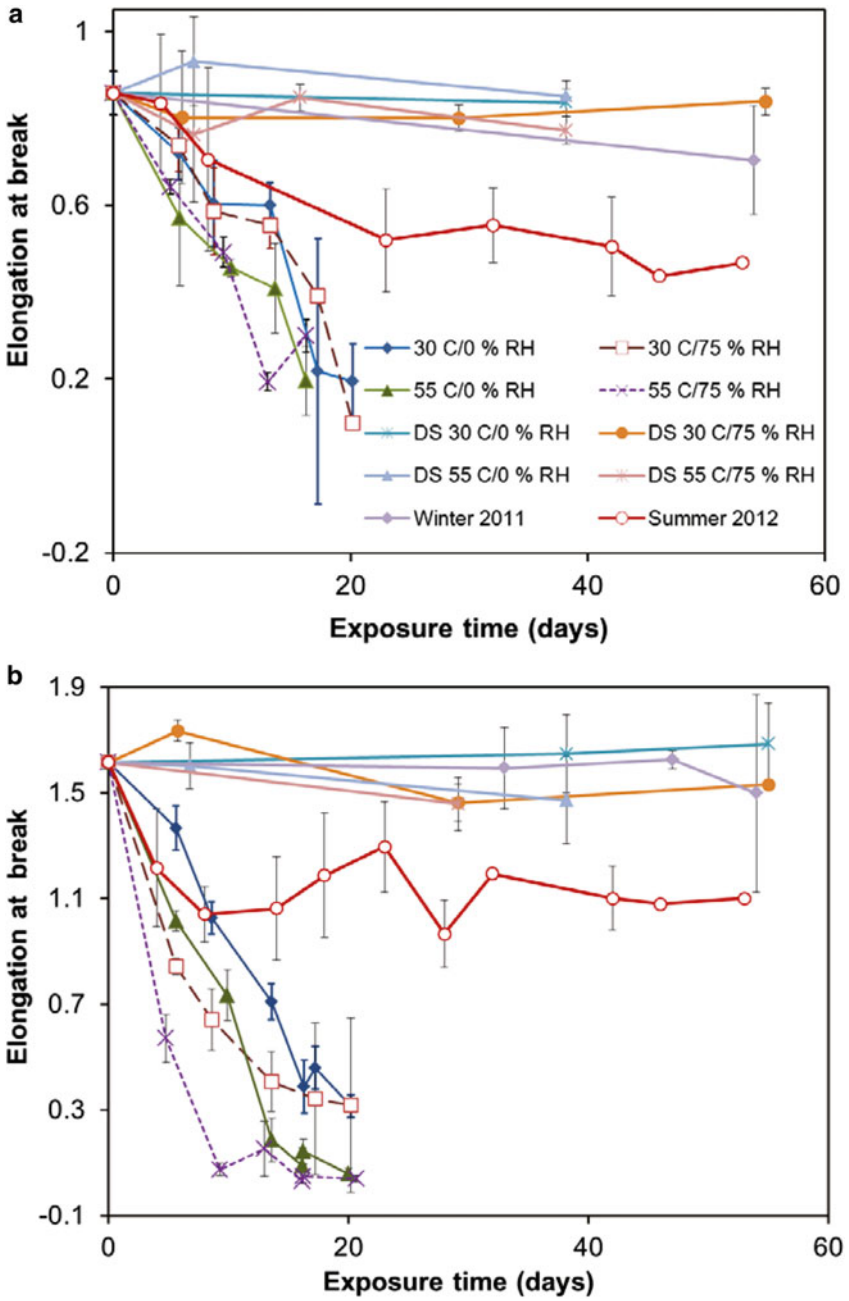

Fig. 15.5 Changes in elongation at break as a function of exposure time for various conditions for (**a**) Films A and (**b**) B. Error bars represent ±1σ from the mean values. "DS" denotes the exposure without UV radiation

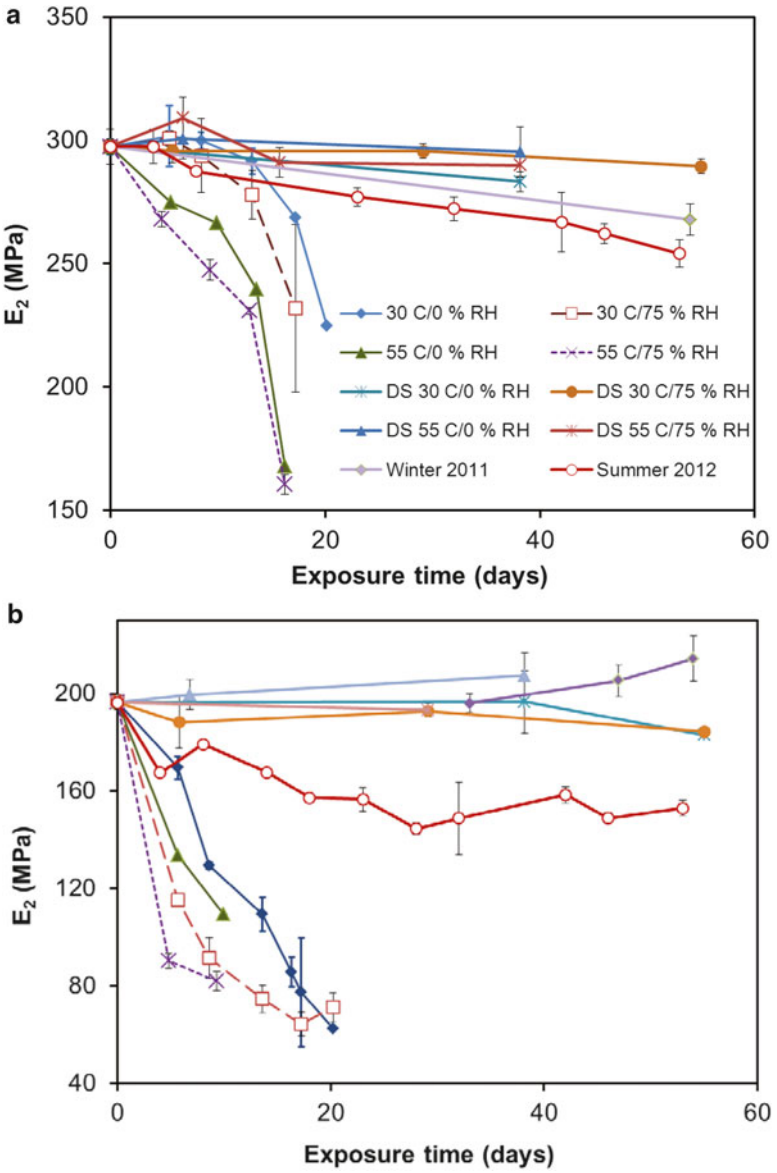

Fig. 15.6 Changes in strain hardening moduli (E_2) as a function of exposure time for various conditions for (**a**) Films A and (**b**) B. Error bars represent ±1σ from the mean values. "DS" denotes the exposure without UV radiation

It is evident that the exposure conditions have dramatic effects on the mechanical properties. The elongation at break precipitously declines with increasing exposure time. To put the matter into perspective, the elongation at break decreases by approximately an order of magnitude after ≈ 10 days of exposure at 55 °C/75 % RH.

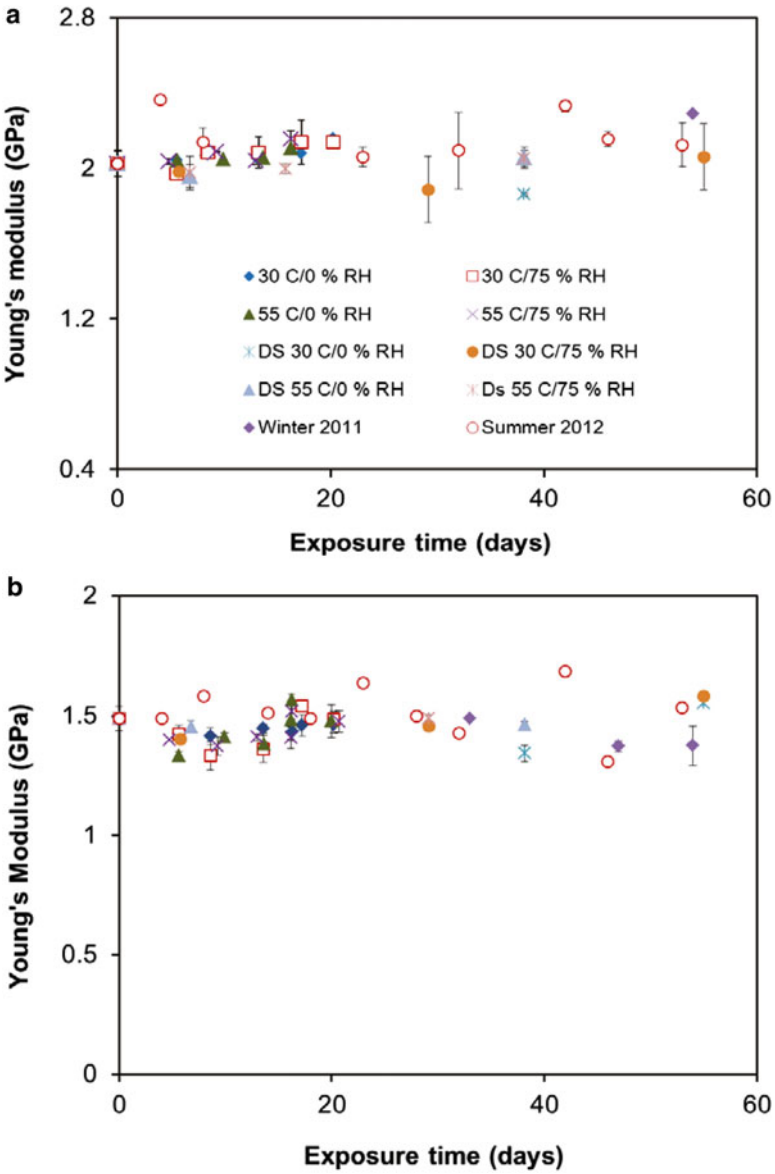

Fig. 15.7 Changes in Young's modulus as a function of exposure time for various conditions for (**a**) Films A and (**b**) B. Error bars represent ±1σ from the mean values. "DS" denotes the exposure without UV radiation

An analogous reduction in strain hardening moduli with increasing exposure times was also observed. After 20 days, the strain hardening for all exposure conditions vanishes. Contemporaneous losses in elongation at break and strain hardening capacity suggest the occurrence of severe localization of strain, which manifests

itself in brittle behavior after exposures. Indeed, this is the case because we observed that failure surfaces of exposed samples were relatively featureless compared to those unexposed samples.

Comparison of the mechanical properties at various exposure times in the absence of UV radiation reveals the weak dependence of degradation on temperature and moisture. In particular, the effect of various combinations of temperature and relative humidity on the elongation at break of Film A is not visibly notable due to large experimental scatters. The rate and the extent of decrease in strain hardening moduli, on the other hand, are found to be slightly greater at 55 °C compared to 30 °C. Unlike Film A, both strain hardening moduli and elongation at break of Film B exhibit marginally greater decreases at high relative humidity at 75 % RH for a given temperature. Also, it is apparent that both elongation at break and strain hardening modulus for Films A and B exposed to a simultaneous high temperature and RH decrease more rapidly than they did for the exposure at various RH conditions and lower temperatures.

As illustrated in Figs. 15.5, 15.6, and 15.7, the degradation of the materials in the absence of UV under the similar temperature and RH combinations is seriously retarded, as indicated by little or no changes in mechanical properties with increasing exposure time. This weak dependence is consistent with the chemical changes occurring in the films, which again underlines that this was primarily a UV-controlled phenomenon.

Interestingly, Young's moduli for all conditions are found to remain statistically unchanged within our experimental timescale, irrespective of exposure conditions (Fig. 15.7). This means that the small-strain property below the elastic limit is largely invariant by the structural changes induced by degradation. A thermo-oxidative study of polypropylene at 90 °C comes to the similar conclusion in that a detrimental effect of aging was found for the large-strain behaviors while the low strain characteristics were essentially preserved [23]. Thus, small-strain measurements may not be useful for monitoring aging behavior.

Large-strain deformation of semicrystalline polymers strongly depends on entanglement network density in the amorphous domains [24, 25]. Increasing the entanglement density leads to a tougher polymer and an increase in the corresponding strain hardening capability. Further, amorphous domains in the polymer are well known to be more labile to oxidation as compared to crystalline regions due to their higher permeability to oxygen. Thus, from the FTIR data and tensile tests, the observed losses in chemical and large-strain mechanical properties may be interpreted as a result of bond scissions occurring in tie molecules in the more oxygen-permeable amorphous domains. This gives rise to formation of low molecular weight fragments with low chain entanglement density.

Finally, photodegradation in PET is known to begin on the surface and then progresses gradually into the bulk [26–28] since that correlates with oxygen concentration. For example, early studies by Blais et al. [26] using ATR-FTIR showed that carboxyl groups formed on UV-irradiated PET films were concentrated mostly on the thin surface layer (thickness ≤ 1 μm) and the sample interior was largely unaffected. Consistent with this notion, depth profiling of 200 μm thick PET films using

a micro-FTIR spectroscopy reveals surface enrichment of carboxyl groups, which are distributed heterogeneously only on the sample outermost surface (≤50 μm) after 100 h of polychromatic irradiation with wavelengths greater than 300 nm [27]. The surface-mediated degradation in our samples is confirmed by exposing the adhesive side of the safety films to the UV light source, and the chemical changes on the back face of the samples were followed with ATR-FTIR. After 1 month of exposure, degradation is observed to occur mostly on the irradiated layer of the sample and the back face is unaffected. On the basis of this observation and the foregoing considerations, it is surmised that crazes induced by this surface degradation may serve as initiation sites for failure, causing the degraded film to lose their load-bearing capacities. The proposed mechanism is in line with the literature where the surface degradation is sufficient to cause plastic instability necking and polymers embrittlement even if the bulk polymer is unaffected [29, 30].

Yellowing upon Exposure

UV–visible spectra were collected for degraded materials as well as for fresh materials prior to exposure. Films A and B were found to absorb nearly all of the UV radiation. This is due to the fact that PET is a very strong UV absorber, itself. Moreover, the safety films studied here contain commercial UV absorbers, which are commonly incorporated in the adhesives and/or impregnated in to the polyester film. The extent of yellowing during the period of exposure was evaluated using yellowness index. As shown in Fig. 15.8, changes in the yellowness index could be measured, yet neither of the PET films had any visually delectable yellowing. Typical values for a visually detectable change in yellowing are greater than 100. The values shown in Fig. 15.8 are a maximum of 35 or 14, well short of the visually detectable threshold. Figure 15.8 shows the time evolution of yellowness index for various conditions. It can be seen that Films A and B exhibit increases in yellowness indexes upon exposure. Such discoloration may be related to hydroxylation of the terephthalate ring [12, 31].

Comparison with Field Exposures

An interesting question is how the intense but short-term exposures used in this study can be translated to much less severe field exposure conditions over longer periods of time. To answer this question, correlation plots between 1,724 cm^{-1} and 1,158 cm^{-1} for the field exposures are compared with the equivalent data from the accelerated exposures. As shown in Fig. 15.2, all data points for various environments fall near a single normalized curve, indicating similar degradation mechanism operating in the field and controlled laboratory environments. Such a strong correlation between the accelerated and field exposures may be attributed to the fact that UV radiation between 295 and 400 nm in the sunlight is known to be

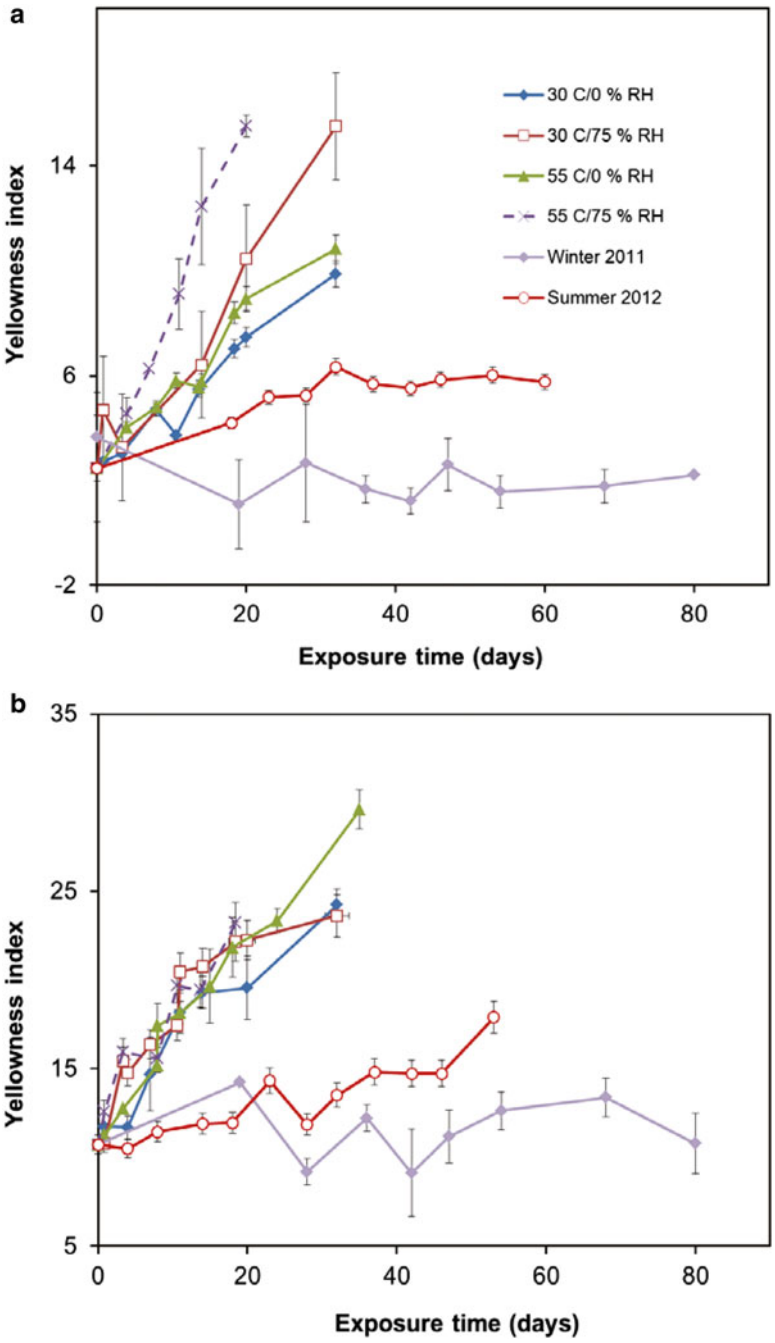

Fig. 15.8 Yellowness indexes for (**a**) Films A and (**b**) B exposed to various conditions. Error bars represent ±1σ from the mean values

photolytically active in degrading polymeric materials [32, 33], and the artificial light source used in the accelerated experiments consists of radiation that is rich in the same wavelength range. Moreover, the combinations of temperature and RH used in the accelerated tests are within the range seen in outdoor exposure conditions, thus precluding deleterious side effects from these variables. For this reason, meaningful comparisons may be made in this study using the data generated under the accelerated and field exposures. As expected a comparison between accelerated and field exposures shows that specimens aged in the field condition have much slower degradation rates both in terms of chemical and mechanical properties (see Figs. 15.3, 15.5, 15.6, and 15.7, respectively).

In the case of yellowing, the films exposed to outdoor show a very low yellowness index, indicating that the degradation is not exhibited by specimen discoloration. Visual inspection fails to reveal any significant changes after outdoor exposure. These results clearly emphasize that while a conventional descriptive methodology involving visual evaluations of physical performance of exposed specimens for defects including color change, crack size, and distribution may relate a customer-perceived failure mode, it is not sensitive to changes that resulted from degradation and provides little insight into the mechanisms leading to these macroscopic changes. This makes it difficult to develop models for accurately predicting the service life of the polymeric films based on visual observation.

In contrast, there is a significant change in the mechanical properties during both the controlled and outdoor exposures. This is especially apparent in the elongation to break data of Fig. 15.5. Developing a model for accurately predicting the service life of the polymeric films based on changing mechanical properties would be relatively straightforward.

Conclusions

Indoor accelerated and field weathering of two polymeric films used in protective glazing systems has been studied using FTIR spectroscopy, ultraviolet–visible spectroscopy, and tensile tests. Accelerated exposures led to the formation of hydroxyl and carboxyl functional groups on the surface of specimens. Substantial decreases in elongation at break and strain hardening modulus with increasing exposure time were observed while the Young's modulus remains largely unaffected within the experimental timescale. These results demonstrate the insensitivity of the small-strain properties to weathering. Prolonged exposures render specimens brittle, diminishing the mechanical integrity of the polymers through extensive chain scissions. Degradation of the polymers was found to be predominately controlled by UV radiation, while temperature and moisture contents play only a secondary role. Finally, the samples exposed to the outdoor conditions degraded in the same way as they did when subjected to the accelerated conditions, but at much slower rates.

Acknowledgment AL and PG acknowledge the Summer Undergraduate Research Fellowships at National Institute Standards and Technology.

References

1. Jacques LFE (2000) Prog Polym Sci 25:1337–1362
2. Schnabel W (1982) Polymer degradation, principle and practical applications. MacMillan, New York
3. Chin J, Byrd E, Embree N, Garver J, Dickens B, Finn T, Martin J (2004) Rev Sci Instrum 75:4951–4959
4. Colthup NB, Daly LH, Wiberley SE (1990) Introduction to infrared and Raman spectroscopy, 3rd edn. Academic, San Diego
5. Gu X, Raghavan D, Nguyen T, VanLandingham MR, Yebassa D (2001) Polym Degrad Stab 74:139–149
6. Liang CY, Krimm S (1959) J Mol Spectrosc 3:554–574
7. Boerio FJ, Bahl SK, McGraw GE (1976) J Polym Sci Polym Phys Ed 14:1029–1046
8. Bahl SK, Cornell DD, Boerio FJ, McGraw GE (1974) J Polym Sci Polym Lett Ed 12:13–19
9. Miyake A (1959) J Polym Sci 38:479–495
10. Shi W, Qu B, Ranby B (1994) Polym Degrad 44:185–191
11. Holland BJ, Hay JN (2002) Polymer 43:1835–1847
12. Edge M, Wiles R, Allen NS, McDonald WA, Mortlock SV (1996) Polym Degrad Stab 53:141–151
13. Day M, Wiles DM (1972) Can Text J 89:69
14. Rabek JF (1987) Mechanisms of photophysical processes and photochemical reactions in polymers. Wiley, New York, p 534
15. Kamal MR, Huang B (1992) In: Hamid SH, Amin MB, Maadhah AG (eds) Handbook of polymer degradation. Dekker, New York, pp 127–168
16. McNeill IC, Bounekhel M (1991) Polym Degrad Stab 34:187–204
17. Sivasamy P, Palaniandavar M, Vijayakumar CT, Lederer K (1992) Polym Degrad Stab 38:15–21
18. MacDonald WA (2002) Polym Inter 51:923–993
19. Samperi F, Puglisi C, Alicata R, Montaudo G (2004) Polym Degrad Stab 83:11–17
20. Sammon C, Yarwood J, Everall N (2000) Polym Degrad Stab 67:149–158
21. Seo KS, Cloyd JD (1991) J Appl Polym Sci 42:845
22. Ballara A, Verdu J (1989) Polym Degrad Stab 26:361–374
23. Fayolle B, Audouin L, Verdu J (2000) Polym Degrad Stab 70:333–340
24. Tervoort TA, Govaert LE (2000) J Rheol 44:1263–1277
25. van Melick HGH, Govaert LE, Meijer HEH (2003) Polymer 44:2493–2502
26. Blais P, Day M, Wiles DM (1973) J Appl Polym Sci 17:1895–1907
27. Grossetete T, Rivaton A, Gardette JL, Hoyle CE, Ziemer M, Fagerburg DR, Clauberg H (2000) Polymer 41:3541–3554
28. Hurley CR, Leggett GJ (2009) ACS Appl Mater Interfaces 1:1688–1697
29. Carlsson DJ, Wiles DM (1971) Macromolecules 4:179–184
30. So PK, Broutman LJ (1982) Polym Eng Sci 22:888–894
31. Ciolacu CFL, Choudhury NR, Dutta NK (2006) Polym Degrad Stab 91:875–885
32. Martin JW (2002) In: Martin JW, Bauer DR (eds) Service life prediction: methodology and metrologies. American Chemical Society, Washington, DC, pp 2–22
33. Pospisil J, Pilar J, Billingham NC, Marek A, Horak Z, Nespurek S (2006) Polym Degrad Stab 9:417–422